Nuclear Instruments and Methods in Physics Research B 269 (2011) 1992–1996

Contents lists available at ScienceDirect

Nuclear Instruments and Methods in Physics Research B

journal homepage: www.elsevier.com/locate/nimb

# The Columbia University proton-induced soft X-ray microbeam

Andrew D. Harken *, Gerhard Randers-Pehrson, Gary W. Johnson, David J. Brenner

*Center for Radiological Research, Columbia University, New York, NY 10032, USA*

ARTICLE INFO

*Article history:*
Received 23 December 2010
Received in revised form 27 May 2011
Available online 2 June 2011

*Keywords:*
Soft X-ray
Microbeam
PIXE

ABSTRACT

A soft X-ray microbeam using proton-induced X-ray emission (PIXE) of characteristic titanium ($K_\alpha$ 4.5 keV) as the X-ray source has been developed at the Radiological Research Accelerator Facility (RARAF) at Columbia University. The proton beam is focused to a 120 μm × 50 μm spot on the titanium target using an electrostatic quadrupole quadruplet previously used for the charged particle microbeam studies at RARAF. The proton induced X-rays from this spot project a 50 μm round X-ray generation spot into the vertical direction. The X-rays are focused to a spot size of 5 μm in diameter using a Fresnel zone plate. The X-rays have an attenuation length of (1/*e* length of ~145 μm) allowing more consistent dose delivery across the depth of a single cell layer and penetration into tissue samples than previous ultrasoft X-ray systems. The irradiation end station is based on our previous design to allow quick comparison to charged particle experiments and for mixed irradiation experiments.



## 1. Introduction

Microbeam irradiators have been developed to study the effects of radiation on single cells and the non-targeted cells around them [1–3]. While most of this work has focused on charged particles, interest has developed on the effects of X-rays on this same scale [4,5]. We have developed a 5 μm soft X-ray microbeam system base on proton induced X-ray emission (PIXE) that produces an X-ray beam with the photon energy of 4.5 keV (Ti-$K_\alpha$) at the Radiological Research Accelerator Facility (RARAF) at Columbia University. This energy is between the typical ultrasoft X-ray systems that operate in the 'water window' (280–500 eV) [4] and the energies typically used at synchrotrons (5–100 keV) [5] and broad beam irradiators of hard X-rays (50 keV and greater).

The long attenuation length (1/*e* is ~145 μm) of the 4.5 keV Ti-$K_\alpha$ X-rays will also make this an ideal tool for studying effects of localized irradiation of specific targets at depth in a tissue sample. This targeted irradiation is not available with lower energy X-rays as they will be absorbed in the initial layers of a tissue. Particle beams also cannot provide the depth targeting available here as the particles will scatter in the tissue losing their focused properties and irradiate many cells in the area making irradiated to non-irradiated distinctions difficult if not impossible. This X-ray energy, while still have good penetration characteristics for irradiating multiple layers into a tissue, also has enough absorbance in a single cell layer to deliver a required dose in a short period of time unlike higher energies. The single layer dose will have an even distribution across the thickness of a cell, unlike carbon X-rays which have a dose variation of nearly 30% across a cell thickness.

Soft X-rays are a well characterized form of radiation that causes specific types of damage to DNA and cellular structures [6]. This characterization has happened in broad beam irradiations of many cells simultaneously and, in the past 10 years, has come under single cell studies with the development of soft X-ray microbeams [4,5]. The types of damage seen from soft X-rays are similar to that of high-LET radiation but limited to localized regions. Most high-LET radiation sources are heavy energetic particles with ionization tracks that are several micrometers wide and typically 10s of micrometers long, usually traversing a whole cell creating a distribution of damage throughout the cell. Soft X-rays, on the other hand, are typically absorbed and generate a single free electron at the absorption location with a track typically less than a micrometer. These localized effects can have distinct effects on certain aspects of cells while allowing most of the cell to continue without any effect. This soft X-ray microbeam, with photon energy of 4.5 keV, will produce secondary electron tracks of range of ~400 nm presenting an average LET of 12.5 keV/μm. The traditional transition point from low to high LET regimes is 10 keV/μm, thus the PIXE microbeam will be directly probing the effects in this region. Soft X-rays, as they are absorbed, have very little scatter and short secondary electron lengths, allow a specific part of a cell to be irradiated while not irradiating any other part of the cell or its neighbors allowing evaluation of that cell and potential bystander effects in neighboring cells.

More recently, these moderate to soft energy X-rays are being developed into new apparatus for both medical imaging and homeland security [7]. The different effects of low doses of soft X-rays on

* Corresponding author. Address: RARAF, 136 S. Broadway, P.O. Box 21, Irvington, NY 10533, USA. Tel.: +1 914 591 9244; fax: +1 914 591 9405.
*E-mail address:* adh2121@columbia.edu (A.D. Harken).

0168-583X/$ - see front matter © 2011 Elsevier B.V. All rights reserved.
doi:10.1016/j.nimb.2011.05.033

specific targets and non-targets will have significant input into the widespread use of these new systems and the potential effect on the population at large from these new sources of radiation.

## 2. Materials and methods

The PIXE X-ray microbeam has been designed to use a reflection source where the generated X-rays are emitted from the proton incidence surface similar to most standard X-ray generators. The use of protons instead of high energy electrons leads to a significant reduction in bremsstrahlung background of the X-ray spectrum. This source has been coupled with a biological end station that allows very precise measurement and target locating for the beam verification and irradiation experiments.

### 2.1. Proton beam and proton target

The proton beam at RARAF is generated from a 5.5 MV Singletron accelerator (High Voltage Engineering Europa, Amersfoort, The Netherlands). This accelerator has voltage ripple of less than 100 V and produces the proton beam through an RF plasma ion source. The beam is transported through a vacuum, is collimated by slits and magnetically focused at the proton beam object aperture. The proton beam object aperture is a set of 4 movable vanes that can define the beam as needed for final shape. This work required a square beam of 1.5 mm on a side for adequate focusing. The protons are focused on the X-ray generation target using an electrostatic quadrupole quadruplet which was previously used in the RARAF charged-particle microbeam and has been described elsewhere [8,9]. The leading aperture on the first ground plane of the electrostatic lens limits the angle of acceptance of the beam giving the final focusing parameters in combination with the object aperture. Initial beam alignment and focusing tests were performed by placing a quartz view glass at the titanium target location and optically viewing the fluorescence generated by the proton beam on the quartz.

Titanium was chosen as the target for the PIXE X-ray microbeam for the 4.5 keV (0.276 nm wavelength) characteristic X-rays [10]. This X-ray energy allows significant penetration into biological samples ($1/e$ of $\sim$145 μm) and while still limiting Compton scattering in the specimen delivering most energy to the desired target. The proton energy of 1.8 MeV was selected to avoid the Ti(p,n) reactions, threshold around 2.2 MeV, and allow lower voltages in the electrostatic quadrupole quadruplet for focusing of the proton beam. The X-ray generation cross section for protons at 1.8 MeV is 5 times less than the maximum cross section at 9 MeV [10]. However, we are limited by our accelerator to 5 MeV at most which is only two times greater than 1.8 MeV. The X-ray generation at 1.8 MeV will have the characteristic X-rays generated at a rate more than 2 orders of magnitude above that of the bremsstrahlung from the protons slowing in the target [11]. For comparison, an electron gun generation system from titanium will have less than one order of magnitude characteristic generation rate over the bremsstrahlung and there would be greater bremsstrahlung generation than in the proton case [12]. The X-ray generation rate in both methods is highly dependent on particle energy. However, the ratio of bremsstrahlung generation to characteristics X-ray will remain fairly consistent. This significant overall reduction in bremsstrahlung generation as well as the characteristic X-rays to bremsstrahlung ratio in the proton method allows us to effectively ignore the bremsstrahlung generation for the PIXE system reported here.

Aluminum was considered as a potential target as it has an intermediate energy at 1.5 keV and larger generation cross section, but the higher energy of titanium with the subsequent penetration advantage was deemed more advantageous. An aluminum target could be used in the future with a slight modification in the zone plate holder as the focal length would be significantly shorter.

The titanium target is a 6 mm titanium slug embedded in a 2.54 cm copper rod. The copper rod extends out of the vacuum system and is positionally adjustable in depth and rotation to center the titanium target face at the correct orientation for the best X-ray emission. The copper rod will also serve as a heat sink if larger currents are to be used. A preliminary calculation using the modeling software ANSYS [13] showed that for the proton current (500 nA) and proton energy (1.8 MeV) the target would reach a thermal equilibrium of 35 °C with localized heating at the incident spot to 50 °C. This is consistent with observations that the target does not get warm to the touch during operation and there is not observable damage to the target when visually inspected after operation. Further calculation shows that with present radiative cooling only, a current of 5 microamps could be placed on target before localized target temperatures near the proton impingement point would increase to 90% of the target melting point (1668 °C). Active cooling, either through forced air or water, could potentially allow more proton current on target, but the 10-fold increase in beam current is sufficient for the present time.

The titanium target face is cut at a 70° angle to the incident proton beam direction to give X-ray emission in the vertical orientation and provide for sufficient X-ray generation while maintaining a small X-ray generation spot size. The 70° angle was chosen for several reasons. Modeling using SRIM [14] shows that the maximum penetration depth of the protons in Ti is 25 μm, however, due to the incidence angle and self absorption, only a small portion of this total length will produce X-rays that can emit into the vertical direction and be part of the X-ray beam. The X-ray generation spot will be the width of the proton beam with the length determined by the projection of the height on a 70° angle plus the depth X-rays generated sub-surface which can escape out of the target. For spot size estimations, the cut off for the penetration escape edge is where 90% of the X-rays generated at a given depth in the vertical direction escape the target material. Therefore, an approximate 100 μm round proton beam will theoretically have an oblong X-ray generation spot of 100 μm × 50 μm, while a 20 μm round proton beam which will give a more round projection of 20 μm × 23 μm. Fig. 1 is a comparison of the proton incidence angle to the generated X-ray spot size for several sizes of proton focus sizes while Fig. 2 is the relation between incidence

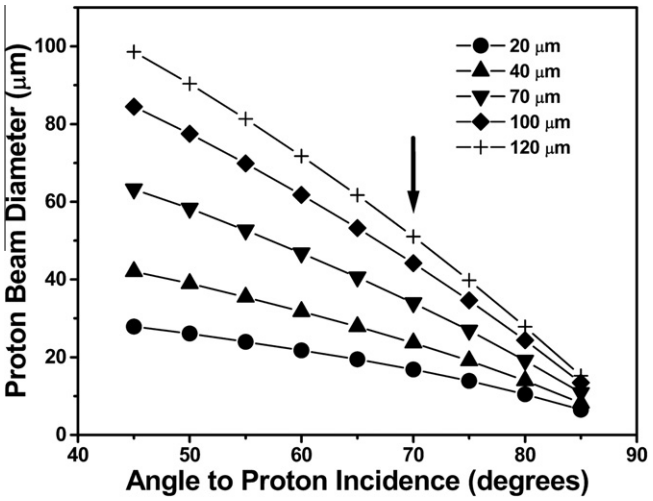


**Fig. 1.** Calculated projected X-ray spot sizes in the vertical direction for varying angle of the titanium incidence face to the proton beam and varying the proton beam spot size. 70° was ultimately chosen for this work.

angle and X-ray generation rate in photons per proton at 1.8 MeV. Ideally, one would want to be to the right and down in Fig. 1 and to the left and upon Fig. 2. Fig. 1 influences the selection of the desired proton spot size as the projection of that spot size onto the angled target will determine the size of the X-ray generation spot presented to the zone plate for focusing. Fig. 2 is most directly related to the self absorption of the generated X-rays by the target material. X-rays generated sub surface have a probability of being absorbed in the material vertically above the generation point before exiting the target and becoming part of the vertical X-ray beam. These competing factors lead to the choice of a 70° titanium target face to proton incidence angle with a proton beam 50 μm width × 120 μm height projecting into a 50 μm × 50 μm spot generating 0.017 photons per proton at the target face. The X-ray zone plate focusing optics will generate an X-ray beam focus of ~5 μm diameter from this source with an expected beam rate of 5–10 photons/s at the focus.

### 2.2. X-ray optics

A Fresnel zone plate was chosen as the X-ray focusing optic of the PIXE soft X-ray microbeam. A zone plate is a diffractive optic consisting of concentric opaque and transparent rings that get smaller as the radius increases [15]. Zone plates, as diffractive optics, are limited to monochromatic energy situations. Proton induced X-rays have very little bremsstrahlung generation [10] and can be considered a monochromatic source for this project making the use of a zone plate practical. The focal length of a zone plate lens ($f$) is determined by the wavelength to be used ($\lambda$), the number of rings ($N$), and the outer most ring diameter ($\Delta r$).

$$f = 4N\frac{\Delta r^2}{\lambda} \quad (1)$$

As this is a diffractive optic, there will be several orders of diffraction. The calculated focal length in (1) is for the first order; the 3rd and higher orders will focus closer to the zone plate and are disposed of on the center stop and the order selecting exit aperture. The zone plate was chosen to have an overall diameter of 120 μm, an outer most ring width of 50 nm and a total of 600 diffracting rings giving a focal length of 21.7 mm at 0.276 nm wavelength. A stainless steel center stop 25 μm in diameter and 75 μm thick was selected in combination with a 25 μm order selecting aperture. The distance from the X-ray generation spot to the zone plate was 250 mm giving a focus point at 23.8 mm above the zone plate with the order selecting aperture placed 100 μm below that point. This gives the zone plate an expected demagnification of 11 producing a spot size just below 5 μm from the projected proton beam spot of 50 μm. The zone plate was purchased from ZonePlates, Ltd., (London, UK) and the focusing efficiency has been measured by the manufacturer to be 12.4%.

The long focal length of the zone plate of nearly 24 mm gives a deep geometric depth of field. The X-ray focal spot of 5 μm will expand at a rate of 2.4 μm/mm. This gives, at minimum, a 6 μm X-ray beam over a depth of 0.8 mm. This depth of field for beam size is sufficient for current experiments targeting cell nuclei which are on the order of 10–12 μm.

Fig. 3 is a schematic of the end station construction with the X-ray focusing optics from the titanium target to the samples on the microscope stage. The main features are the titanium target in the vacuum system at the proton beam level, a 25 μm think beryllium vacuum window and a helium-filled cylinder in which the zone plate is mounted with a custom $x$–$y$ adjustment stage. The total length from the titanium target to the sample is 27.3 cm. The beryllium window (6 mm in diameter and 10 cm from the titanium target) with the helium filled cylinder allows the transmission of the X-rays with minimal losses (<2%) to the sample while stopping any backscattered protons from reaching the zone plate. The X-ray focusing optics column is separately supported from the microscope/stage assembly allowing the sample position and microscope optical focus point to be adjusted relative to the X-ray focus point. A scintillation window was placed at the location of the titanium target and the proton beam spot was visually measured to be near this desired ellipse of 50 μm × 120 μm. This visualization also confirmed the proton spot to zone plate distance to be 249 mm. This results in the zone plate focusing 10 μm closer than calculated but is negligible compared to the depth of field. The order selecting aperture is fixed by design with the top surface at 23.7 mm from the zone plate. The focal point for the microscope/stage end station was placed optically 100 μm above that location.

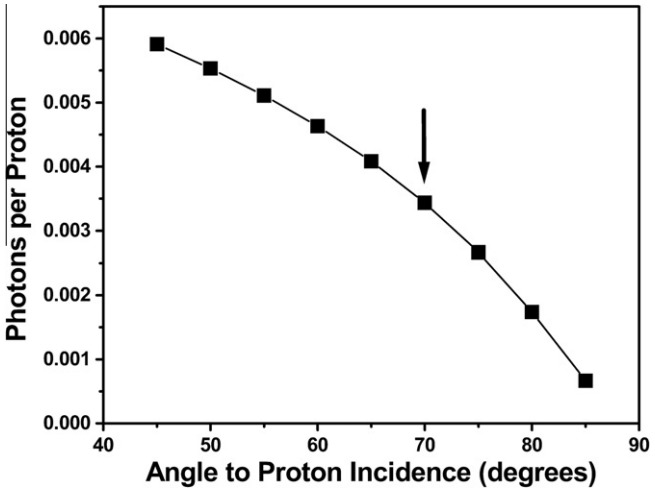


**Fig. 2.** Calculated X-ray generation rate projected into the vertical direction per incident proton on the titanium target with the proton energy of 1.8 MeV. 70° was ultimately chosen for this work.

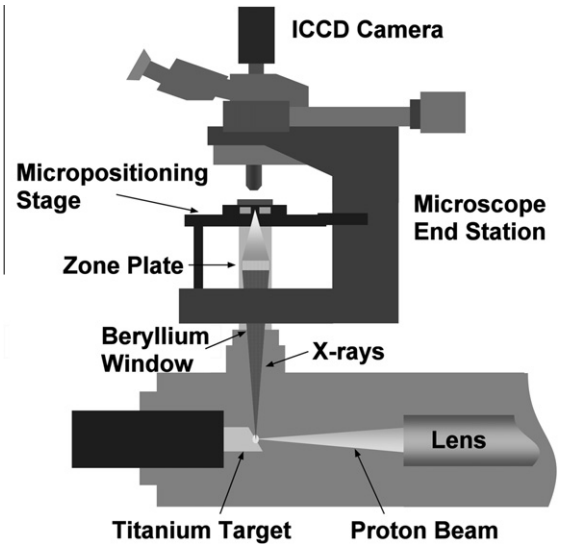


**Fig. 3.** Schematic diagram of the X-ray microbeam end station. The proton beam enters the lens from the right, is focused by the lens, and impinges on the titanium target generating X-rays. The X-rays pass vertically out of the vacuum through a beryllium window into a helium filled transmission tube holding the zone plate. The X-rays leave the transmission tube through the order selecting aperture which is 100 μm below the irradiation sample on the micropositioning stage.

### 2.3. Biological end station

The biological end station is based on our previous designs [16]. The X-ray beam is oriented in the vertical direction so that the specimen dishes can be horizontal allowing the use of existing microbeam dish designs for irradiation. The end station, schematically shown in Fig. 3, is composed of a Nikon FN1 fluorescence microscope (Nikon USA, Melville, NY, USA), a combination high precision stage (Microstage with Nano-Z stage, MadCity Labs, Madison, WI, USA), and an intensified CCD camera (Pulnix, JAI Inc, San Jose, CA, USA). This combination allows precision (~1 μm) locating of measurement devices and irradiation samples as well as high quality imaging for sample recognition and targeting. The end station is mounted on a custom stand at the end of the horizontal beam line at RARAF. The housing of the electrostatic quadruple quadruplet is integrated as part of the custom stand to assist in the ultimate alignment of all the optics.

Beam diagnostics are performed with a detector mounted to the objective of the microscope. However, the absorption of the X-rays in the sample makes it impractical to have a beam diagnostic detector above the samples during irradiation. Monitoring of the beams (proton and X-ray) during irradiation is performed by monitoring the proton beam current on the target and an X-ray detector (XR100, AMPTEK Inc., Bedford, MA, USA) placed off at an angle (72°) to the irradiation beam in a position to monitor the X-ray generation rate. The stability of the system is such that a single check of the X-ray beam location, proton beam current, and calibration to the monitor at the beginning of an irradiation is sufficient to verify dosimetry for the irradiation. This monitoring system allows medium to be left on the cells during irradiation giving the samples less exposure to the room environment compared to the current charge particle systems. The medium also allows for the longer exposures required from the currently lower dose rate.

## 3. Results and discussion

An order selecting aperture is required when using a diffractive optic to eliminate the diffraction orders that are not contributing to the microbeam focus. For this system a 25 μm OSA was selected to be used. The 3rd order diffraction ring projected from the center stop will be 75 μm in diameter at the OSA plane and will be completely eliminated. The alignment of the OSA with zeroth (non-diffracted) order center stop is critical for the X-ray microbeam as any undiffracted beam could irradiate a cell outside the focal point. The OSA is mounted at the top of the X-ray optics column seen in Fig. 3 and is positioned using micrometric screws to align to the focused beam. When the focused beam is in the center of the aperture, it will be aligned with the center stop which will be observable as no beam outside the center focus will be present. Verification of this alignment is performed as part of the knife edge scans for spot size measurement.

The measurement of the X-ray focus spot size was performed using the standard knife-edge occlusion method. For this method, a knife edge of suitable material is passed through the focal point of the beam in front of a detector. The material must be of sufficient density to affect the beam in a measurable way while still being thin enough to not distort the beam characteristics. The measurable change in detection rate determines the amount of beam occluded. The knife edge is stepped through the beam and a profile is generated of the beam occlusion rates at each step. The knife edge material chosen was 30 μm of gold as this would stop all of the X-rays that impact the surface and is sufficiently thin compared to the near millimeter of geometric depth of field for this beam. Fig. 4 shows the resulting passes in two orthogonal directions with the beam spot size of 5 μm × 5 μm. This measurement

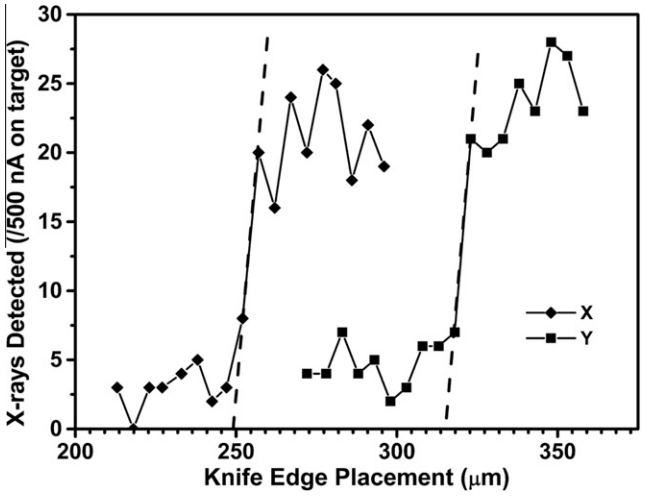


**Fig. 4.** Orthogonal knife edge scans of the X-ray focus spot. These transitions show the beam is 5 μm × 5 μm. The *X* direction corresponds to the 50 μm proton beam width and the *Y* direction corresponds to the 120 μm proton height, projected vertically as 50 μm, from the titanium target.

is consistent with the proton spot size of 50 μm by 120 μm which is close to predicted and observed proton beam sizes.

While larger than the typical charged-particle microbeams at RARAF, the 5 μm X-ray beam is sufficiently small for performing irradiations of cell nuclei. Further development of this system will be for improved focusing of the proton beam to smaller sizes resulting in smaller X-ray focus spots.

The current dose delivered to a single cell will be 1 mGy/s based on a 10 μm spherical cell absorbing 1 photon/s. While sufficient for current studies, this dose rate will be increased as improvements to the proton and X-ray beams are performed for the ultimately smaller spot sizes.

## 4. Conclusions

We have developed a soft X-ray microbeam for irradiation of biological samples using proton induced X-ray emission (PIXE) as the soft X-ray source from characteristic titanium X-rays of 4.5 keV. Using an electrostatic quadruple quadruplet, the proton beam is focused onto the titanium target to produce X-rays in a 50 μm spot projected into the vertical direction. A Frensel zone plate is used to focus the X-rays to a final spot of 5 μm in diameter. The ongoing development of this irradiation system will result in higher beam rates for more throughput and more focusing of the proton beam to create smaller X-ray spots sizes for sub-cellular target irradiations.

## Acknowledgements

The authors thank Yanping Xu for his assistance with the ANSYS modeling. This work was sponsored by a P41 grant for the National Institute of Biomedical Imaging and Bioengineering (NIBIB): 2 P41 EB002033-14.

## References

[1] G. Randers-Pehrson, C.R. Geard, G. Johnson, C.D. Elliston, D.J. Brenner, The Columbia University single-ion microbeam, Radiat. Res. 153 (2001) 210–214.
[2] M. Folkard, B. Vojnovic, K.M.B. Prise, A.G. Bowey, R.J. Locke, G. Schettino, B.D. Micheal, A charged-particle microbeam: I. Development of an experimental system for targeting cells individually with counted particles, Int. J. Radiat. Biol. 72 (1997) 375–385.
[3] M. Heiβ, B.E. Fischer, B. Jakob, C. Fournier, G. Becker, G. Taucher-Scholz, Targeted irradiation of mammalian cells using a heavy-ion microprobe, Radiat. Res. 165 (2006) 231–239.

[4] M. Folkard, G. Schettino, B. Vojnovic, S. Gilchrist, A.G. Michette, S.J. Pfauntsch, K.M. Prise, B.D. Micheal, A focused ultrasoft X-ray microbeam for targeting cells individually with submicrometer accuracy, Radiat. Res. 156 (2001) 796–804.
[5] K. Kobayashi, N. Usami, K. Hieda, K. Takakura, H. Maezawa, T. Hayashi, Development of microbeam irradiation system for radiobiology, Nucl. Instrum. Methods Phys. Res., Sect. A 467–468 (2001) 1329–1332.
[6] D. Goodhead, Inactivation and mutation of cultured mammalian cells by aluminum characteristic ultrasoft X-rays III. Implication for theory of dual radiation action, Int. J. Radiat. Biol. 32 (1977) 43–70.
[7] D. Brenner, E. Hall, Computed tomography – an increasing source of radiation exposure, N. Engl. J. Med. 357 (2007) 2277–2284.
[8] G. Randers-Pehrson, G.W. Johnson, S.A. Marino, Y. Xu, A.D. Dymnikov, D.J. Brenner, The Columbia University sub-micron charged particle beam, Nucl. Instrum. Methods Phys. Res., Sect. A 609 (2009) 294–299.
[9] A.D. Dymnikov, D.J. Brenner, G.W. Johnson, G. Randers-Pehrson, Theoretical study of short electrostatic lens for the Columbia ion microprobe, Rev. Sci. Instrum. 71 (2000) 1646–1650.
[10] J.S. Lopes, A.P. Jesus, G.P. Ferreira, F.B. Gil, X-ray production in Ca, Sc, Ti, V, Cr, Mn and Fe by protons of 0.5–2 MeV energy, J. Phys B: Atom. Mol. Phys. 11 (1978) 2181–2188.
[11] K. Murozono, K. Ishii, H. Yamazaki, S. Matsuyama, S. Iwasaki, PIXE spectrum analysis taking into account bremsstrahlung spectra, Nucl. Instrum. Methods Phys. Res., Sect. B 150 (1999) 76–82.
[12] L. Tian, J. Zhu, M. Liu, A. Zhu, Bremsstrahlung spectra produced by kilovolt electron impact on thick targets, Nucl. Instrum. Methods Phys. Res., Sect. B 267 (2009) 3495–3499.
[13] ANSYS v11, http://www.ansys.com.
[14] SRIM v2008.04, http://www.srim.org.
[15] C.A. MacDonald, W.M. Gibson, X-ray and neutron optics, in: M. Bass, J.M. enoch, E.W.V. Stryland, W.L. Wolfe (Eds.), Handbook of Optics, Vol III Classical, Vision and X-ray Optics, McGraw-Hill, New York, 2001, pp. 19.11–30.17.
[16] A.W. Bigelow, G.J. Ross, G. Randers-Pehrson, D. Brenner, The Columbia University microbeam II endstation for cell imaging and irradiation, Nucl. Instrum. Methods Phys. Res., Sect. B 231 (2005) 202–206.